Technical Report 1275
February 1989

Airborne FLIR Detection of Surface Targets

H. G. Hughes

*Original contains color plates: All DTIC reproductions will be in black and

NAVAL OCEAN SYSTEMS CENTER
San Diego, California 92152–5000

F. G. SCHWEIZER, CAPT, USN
Commander

R. M. HILLYER
Technical Director

ADMINISTRATIVE INFORMATION

This work was performed by the Tropospheric Branch, Code 543, Naval Ocean Systems Center, for the Office of Naval Technology.

Released by
H. V. Hitney, Head
Tropospheric Branch

Under authority of
J. H. Richter, Head
Ocean and Atmospheric
Sciences Division

ACKNOWLEDGMENTS

I wish to thank Fritz G. Wollenweber of the German Geophysical Office, Federal Republic of Germany, who was responsible for incorporating the waveslope statistical model into LOWTRAN 6 and for many helpful discussions. Appreciation is also extended to Douglas R. Jensen, who provided the airborne measurements of meteorological parameters, and to Merle R. Paulson, who assisted in the AGA measurements. John Cook of the Naval Environmental Prediction Research Facility, Monterey, California, was responsible for providing the FORTRAN version of SHIPSIG. Juergen H. Richter was responsible for providing the funding for this work effort.

REPORT DOCUMENTATION PAGE

1a. REPORT SECURITY CLASSIFICATION UNCLASSIFIED	1b. RESTRICTIVE MARKINGS
2a. SECURITY CLASSIFICATION AUTHORITY	3. DISTRIBUTION/AVAILABILITY OF REPORT
2b. DECLASSIFICATION/DOWNGRADING SCHEDULE	Approved for public release; distribution is unlimited.
4. PERFORMING ORGANIZATION REPORT NUMBER(S) Technical Report 1275	5. MONITORING ORGANIZATION REPORT NUMBER(S)
6a. NAME OF PERFORMING ORGANIZATION Naval Ocean Systems Center 6b. OFFICE SYMBOL (If applicable) Code 543	7a. NAME OF MONITORING ORGANIZATION
6c. ADDRESS (City, State and ZIP Code) San Diego, CA 92152-5000	7b. ADDRESS (City, State and ZIP Code)
8a. NAME OF FUNDING/SPONSORING ORGANIZATION Office of Naval Technology 8b. OFFICE SYMBOL (If applicable)	9. PROCUREMENT INSTRUMENT IDENTIFICATION NUMBER
8c. ADDRESS (City, State and ZIP Code) Arlington, VA 22217-5000	10. SOURCE OF FUNDING NUMBERS PROGRAM ELEMENT NO.: 62435N PROJECT NO.: RM35G80 TASK NO.: NO2C/02 AGENCY ACCESSION NO.: DN438 760

11. TITLE (Include Security Classification)

AIRBORNE FLIR DETECTION OF SURFACE TARGETS

12. PERSONAL AUTHOR(S)

H. G. Hughes

13a. TYPE OF REPORT	13b. TIME COVERED	14. DATE OF REPORT (Year, Month, Day)	15. PAGE COUNT
Interim	FROM TO	February 1989	26

16. SUPPLEMENTARY NOTATION

17. COSATI CODES			18. SUBJECT TERMS (Continue on reverse if necessary and identify by block number)
FIELD	GROUP	SUB-GROUP	Forward Looking Infrared (FLIR) system Tactical Decision Aid (TDA)

19. ABSTRACT (Continue on reverse if necessary and identify by block number)

An algorithm is presented for predicting the detection ranges of a surface target by an airborne Forward Looking Infrared (FLIR) system. A case study is presented to demonstrate the vulnerability of a Frigate-class ship to detection by an airborne FLIR during a 5-hour period where the ship's course changed allowing solar heating of different sides of the ship. The results of this study show considerable increases in predicted detection ranges with altitude using the present algorithm over those based on a fixed temperature difference between the target and its background.

20. DISTRIBUTION/AVAILABILITY OF ABSTRACT	21. ABSTRACT SECURITY CLASSIFICATION
☐ UNCLASSIFIED/UNLIMITED ☒ SAME AS RPT ☐ DTIC USERS	UNCLASSIFIED

22a. NAME OF RESPONSIBLE PERSON	22b. TELEPHONE (Include Area Code)	22c. OFFICE SYMBOL
H. G. Hughes	(619) 553-1418	Code 543

DD FORM 1473, 84 JAN

83 APR EDITION MAY BE USED UNTIL EXHAUSTED
ALL OTHER EDITIONS ARE OBSOLETE

SUMMARY

An algorithm is presented for predicting the detection ranges of a surface target by an airborne Forward Looking Infrared (FLIR) system. The total infrared background radiance scene under cloud-free skies is modeled to include the atmospheric path emissions between the target and sensor and the effects of a wind-ruffled sea on the surface emissions and sky radiance reflections.

A model is also introduced of the average temperature of a ship based upon the solar heating effects throughout a specified course, the ambient meteorological conditions, and the viewing angle. Together, these two models allow the range to be determined where the difference between the apparent ship's temperature (i.e., the actual ship temperature degraded by the atmospheric transmittance) and the effective background temperature of the sea surface as viewed from the sensor altitude is equal to the minimum detectable temperature difference of the FLIR.

A case study is presented to demonstrate the vulnerability of a Frigate-class ship to detection by an airborne FLIR during a 5-hour period where the ship's course changed allowing solar heating of different sides of the ship. Study results

The results of this study show considerable increases in predicted detection ranges with altitude using the present algorithm over those based on a fixed temperature difference between the target and its background. Keywords: Surface targets, TDA (Tactical Decision Aids), Thermal targets. (edc)

CONTENTS

FIGURES

FIGURES (continued)

INTRODUCTION

The standoff ranges at which an adversary can detect and/or track a surface ship using passive infrared (IR) sensors is of primary importance for a ship commander to be able to estimate the times allowable for evasive actions against guided weaponry launched at the ship or for the deployment of countermeasures. Algorithms presently operational in the U.S. Navy (CSC, 1986, and STX Corp., 1988) for predicting the performance of an airborne Forward Looking Infrared (FLIR) system operating against a surface target are based upon a fixed temperature difference between a target and its natural background. These algorithms determine the range at which the assumed temperature difference is degraded by the atmospheric infrared transmittance to the minimum detectable temperature difference of the sensor system. This approach neglects the effects of a wind-ruffled sea on the surface emissions and sky radiance reflections and the atmospheric path emission contributions to the total background radiance scene which changes with viewing angle and altitude of the sensor.

In this report, a FLIR detection range algorithm is introduced which includes (1) the three aforementioned contributors to the sea radiance under cloud-free skies to derive (with the Cox-Munk (1954) sea surface wave slope statistical model and the LOWTRAN 6 Kneizys et al., (1983) computer code) a background model which varies with sensor altitude and viewing (zenith) angle, and (2) a model of the average ship temperature based upon solar heating effects throughout a specified course and the ambient meteorological conditions. Together, these two models allow the range to be determined where the difference between the ship's apparent temperature (i.e., the actual ship temperature degraded by the atmospheric transmittance) and the effective background temperature as viewed from the sensor position is equal to the minimum detectable temperature difference of the FLIR. A case study is presented (using an actual course of a Frigate operating off the coast of San Diego, California) to demonstrate the use of the algorithm as a Tactical Decision Aid to predict the vulnerability of a Frigate-class ship to detection by an airborne common module FLIR. During a 5-hour period, the ship's course changed allowing solar heating of different sides of the ship. Supportive airborne FLIR measurements were not available to assess the accuracy of the detection range predictions. However, airborne measurements of meteorological parameters and the sea surface temperature (obtained in the ship's operating area) and surface based measurements of 8- to 12-μm IR sky/sea radiances were used to select and evaluate the background model used in the detection range predictions. Also as radiative temperature measurements on board the ship were not available for comparison with the modeled values, the predicted average temperature for the ship could only be compared to that measured (with corrections for atmospheric effects being taken into account) when the ship passed within about 1.7 km of a calibrated infrared imaging system near the end of the 5-hour cruise at sea. In the following sections, the background radiance model and the ship temperature calculations used to predict the detection range envelopes for the selected ship's course are presented for different altitudes of the FLIR. These detection ranges are then compared to those calculated using a constant temperature difference between the ship and the sea background.

MATHEMATICAL FORMULATION OF BACKGROUNDS

Consider the atmosphere to be composed of a number, n, of isothermal layers characterized by temperature T_i and transmittance $\tau(\nu,i,\mu)$ alcng the optical path traversing the ith layer at angle μ, and ν is the spectral wave number. From Kirchoff's law, the radiance of the ith layer is

$$N(\nu, \mathrm{i}, \mu)_{sk} = [1 - \tau_a(\nu, \mathrm{i}, \mu)]W(\tau_i)/\pi \tag{1}$$

where $\tau_a(\nu,i,\mu)$ is the absorption transmittance and $W(T_i)$ is Planck's blackbody radiation formula. Then the spectral radiance reaching the sea surface through the intervening atmosphere is

$$N(\nu, \mathrm{i}, \mu)_{sk} = \left[\prod_{j=1}^{i-1} \tau(\nu, j, \mu)\right] = [1 - \tau_a(\nu, i, \mu)]\left[\prod_{j=1}^{i-1} \tau(\nu, j, \mu)\right]W(T_i)/\pi \ . \tag{2}$$

Summing the contribution from all layers, the spectral radiance at the sea surface is then

$$N(\nu, \mu)_{sk} = \sum_{i=1}^{n}\left\{[1 - \tau_a(\nu, i, \mu)]\left[\prod_{j=1}^{i-1} \tau(\nu, j, \mu)\right]W(T_i)/\pi\right\}. \tag{3}$$

As shown in figure 1, the radiance is allowed to strike a wave facet on the ocean surface with a Gaussian distribution (Cox and Munk, 1954) of angular tilts α and β in the upwind and crosswind directions, respectively, such that an amount $N(\nu,\mu)'$ is reflected into the sensor at an altitude H_1 within the mth layer. The probability that radiance hits the facet is equal to the probability that the wave slope exists, i.e.,

$$N(\nu, \mu)' = P(S_x, S_y)N(\nu, \mu)_{sk} \tag{4}$$

where

$$P(S_x, S_y) = \frac{1}{(2\sigma_x\sigma_y)EXP\left[0.05\left(\frac{S_x^2}{\sigma_x^2} + \frac{S_y^2}{\sigma_y^2}\right)\right]} \tag{5}$$

and $S_x = \tan\alpha, S_y = \tan\beta$, $\sigma_x^2 = 0.003 + 1.92 \times 10^3 V_c$, $\sigma_y^2 = 3.16 \times 10^3 V_c$, with V_c being equal to the current wind speed in the azimuthal direction Φ with respect to the sensor. Then the total spectral radiance that is reflected from all the wave facets into the line of sight of the detector located in the mth layer is

$$N(\nu, \theta)_{rsk} = \left[\prod_{j=1}^{m-1} \tau(j, \theta)\right]\sum_{\mu} R(\nu, \Omega)P(S_x, S_y)N(\nu, \mu)_{rsk} \tag{6}$$

where $R(\nu,\Omega)$ is the complex reflectivity of seawater at the reflection angle Ω. In the above equations, both μ and Ω are implicit functions of S_x and S_y given by Wollenweber (1988)

$$\cos\mu = (2S_x/A)\cos\theta' \cos\phi + (2S_y/A)\cos\theta' \cos\phi - (B/A)\sin\theta' \quad (7)$$

$$\cos\Omega = (S_x/A)\cos\theta' \cos\phi + (S_y/A)\cos\theta' \cos\phi + (1/A)\sin\theta' \quad (8)$$

where $A = S_x^2 + S_y^2 + 1$, $B = S_x^2 + S_y^2 - 1$ and θ is the sensor's zenith angle at the sea surface reflection point.

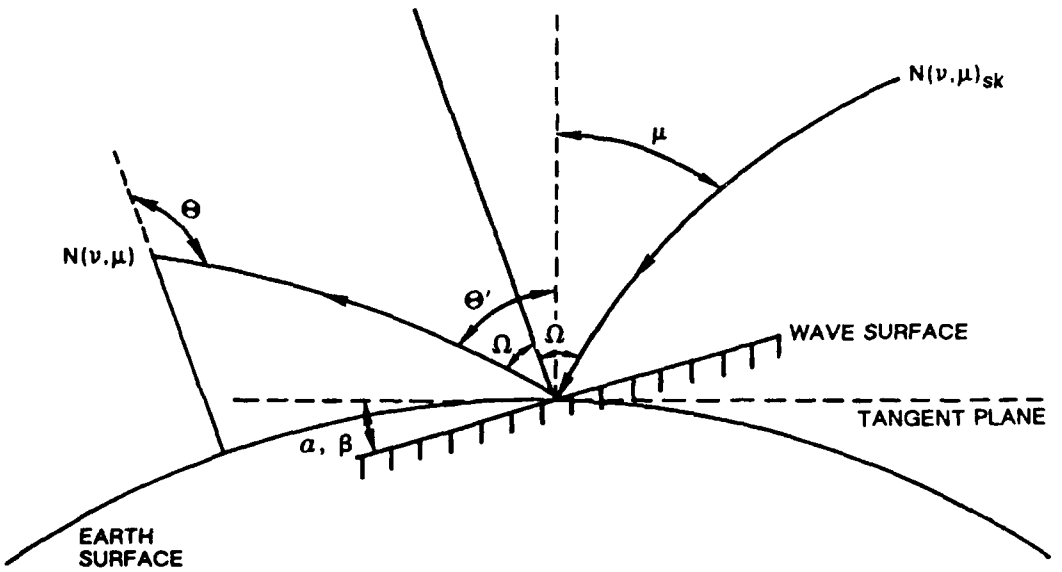

Figure 1. Reflection geometry from a wind-ruffled sea surface.

Similarly, the spectral radiances emitted by the sea surface wave facets (N_{ss}) and the path radiance (N_p), which reach the sensor at the zenith angle θ, are given by

$$N(\nu,\theta)_{ss} = \left[\prod_{j=1}^{m-1} \tau(\nu,j,\theta)\right] \int_{\Omega} P(S_x,S_y)[1 - R(\nu,\Omega)]W(T_{ss})/\pi \qquad (9)$$

and

$$N(\nu,\theta)_p = \sum_{i=1}^{m} [1 - \tau_a(\nu,i,\theta)]\left[\prod_{j=1+1}^{m-1} \tau(\nu,j,\theta)\right] W(T_i)/\pi \qquad (10)$$

where T_{ss} is the sea surface temperature and, again, the angle μ is implicit in the reflection angle Ω.

Then, the total spectral radiance reaching the detector is the sum of the three components

$$N(\nu,\theta)_{tot} = N(\nu,\theta)_{rsk} + N(\nu,\theta)_{ss} + N(\nu,\theta)_p \quad . \qquad (11)$$

The total spectral radiance must then be averaged over the response of the FLIR system which in this case is taken to be the 8- to 12-μm wavelength band. Subroutines have been introduced into LOWTRAN 6 (Wollenweber, 1988) to calculate the total band averaged radiance. The reflection and zenith angles are calculated with equations 5, 7, and 8 corresponding to the incremented values of wave slopes in the intervals $-3\sigma_{x,y} < S_{x,y} < 3\sigma_{x,y}$. To limit the number of calculations, the zenith angles are divided into a maximum of 30 classes (with the criterion that each class should contain at least 10 percent of the probability), and the averaged angles for each class are then used in the radiance calculations.

CALCULATIONS OF BACKGROUND RADIANCE SCENE

For this study, a Piper Navajo aircraft, equipped with Rosemount temperature and pressure probes, and an EG&G dewpoint sensor made a vertical spiral over the ocean to obtain the profile of temperature, relative humidity, and pressure, which are required inputs to the LOWTRAN 6 computer code for calculating the sea and sky radiances. A Barnes PRT-5 radiation thermometer was also on board the aircraft for measurement of the sea-surface temperature from low-level, constant-altitude flights. The vertical profiles of temperature and relative humidity, which were measured at 1330 PST approximately 9 km off the coast of San Diego, are shown in figure 2. The sea-surface temperature measured during this period was 16.4°C. The profiles extending up to an altitude of 2700 m were divided into 33 layers as allowed by LOWTRAN 6. The lower layers of the profiles are also divided into sublayers containing the same amount of absorbing and scattering material and the temperature as the original layer. This artificial layering has been found necessary (Wollenweber, 1988) to remove the anomalous dip (Hughes, 1987), which occurs when aerosols are included in the LOWTRAN 6 radiance calculations for zenith angles close to 90°. The LOWTRAN 6 aerosol model chosen for the calculations is the Navy Maritime Aerosol Model. This model is the sum of three lognormal size distributions and, in addition to the surface wind speeds (current and 24-h averaged) and relative humidity, requires

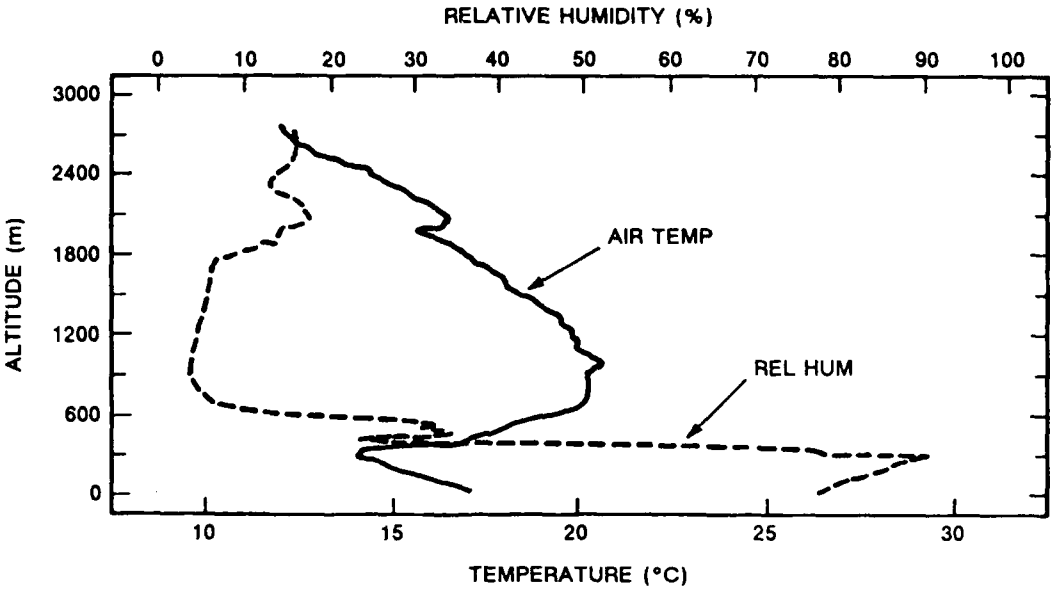

Figure 2. Profiles of air temperature and relative humidity measured with altitude on 9 June 1988 off the coast of San Diego, California.

the input of an air mass factor which identifies the origin of the aerosols as either marine or continental and is allowed to range between integer values of 1 for open ocean to 10 for coastal regions. Also, when an observed surface visibility is available as an input, the model is adjusted so that the calculated visibility at a wavelength of 0.55 μm is the same as the observed value. The air mass factor is defined in terms of atmospheric radon content or an air mass trajectory analysis to determine the time the air mass has been over land. As neither of these techniques were available, an alternate method was used to select an appropriate air mass factor. Near the time that the meteorological parameters were obtained, measurements of IR (8 to 12 μm) horizon radiances were made with a calibrated thermal imaging system (AGA THERMOVISION, model 780) using a 2.95° field-of-view lens with an instantaneous field of view of 0.87 mr. The response of the system was determined by placing a blackbody of known temperature (± 0.1°C for temperatures <50°C) in front of the lens aperture. The digitized video signal transfer function of the system then allowed the blackbody temperature to be reproduced to within ± 0.2°C. For these measurements, the scanner was located at an elevation of 30 m on the Point Loma peninsula in San Diego and was directed in a southerly direction over the ocean such that approximately half of the field of view was above and half below the horizon. The measured radiance scene is shown in figure 3. The data processing software of the AGA system allows the effective blackbody temperature of each pixel in the scene to be displayed on the computer terminal screen and, in this case, the horizontal cursor is situated on the pixel corresponding to the maximum temperature (16.5°C or 3.23 mW/cm² sr) in the scene which is taken to coincide with the infrared horizon. The

temperatures of the different colors in the scene are also identified by the color bars displayed on the left which correspond to the midpoints of the temperatures printed above and below each bar. Using the current and 24-h averaged wind speeds (V_c = 2.9 m/s and ∇ = 2.8 m/s) measured on shore and the vertical profiles of meteorological parameters measured by the aircraft, LOWTRAN 6 calculations were made to agree with the maximum pixel radiance in the scene using nonunique combinations of air mass factors and visibilities. (Note that these calculations were made using a modified current wind speed component, $A_3 = 10^{(0.06V_c - 2.8)}$, which is different from the value published in LOWTRAN 6. This modification was found to be necessary to match previously published measurements of IR sky radiances and near-surface, aerosol size distributions (Hughes, 1987) using the model.) As the AGA scanner could not accurately be plumbed, the zenith angle of the infrared horizon was taken be 0.01° less than the angle for which the LOWTRAN calculations indicated the refracted ray path first hit the earth. In this case, the zenith angle corresponding to maximum radiance is 90.17°. In figure 4 the solid line represents the locus of points which allows the LOWTRAN calculations to match the measured horizon pixel radiance with the different combinations of air mass factors and visibilities. At the time of the measurements, Los Coronados coastal islands off San Diego were barely visible to the naked eye at ranges between 25 and 35 km. In the figure, the integer values of 3 and 4 correspond to visibilities close to these ranges of 23 and 37 km respectively. Figure 5 shows the comparison of the measured and calculated IR radiances for zenith angles within about 1° above and below the horizon using an air mass factor of 3 and a visibility of 37 km. Both the calculated sky ($\theta < 90.17°$) and sea ($\theta > 90.17°$) radiances are in good agreement with the measured values for this low-wind speed case. Whether or not similar agreements can be obtained for higher wind speed conditions needs to be determined.

Using the selected atmospheric model, the contributions of the path, sea, and reflected sky radiances to the total background radiance were calculated as a function of altitude and zenith angle. In figure 6, an example is presented of the calculations for a sensor altitude of 1000 m. For zenith angles less than about 95°, note that the major contribution to the background is the path emission with the reflected sky radiance being less than 10 percent of the total. These relative contributions will, of course, change for other altitudes. In figure 7 the total apparent blackbody temperature of the sea background from the three contributors is plotted versus zenith angle for sensor altitudes of 500 and 2000 m. At the 500-m elevation, the dip in temperature at about 97° is a result of the rapid fall off of path emission with increasing zenith angle (i.e., shorter slant paths to earth than at the 2000 m). For zenith angles greater than about 100°, there is little difference in the apparent temperatures at each altitude and both approach the measured sea-surface temperature at the nadir zenith angle.

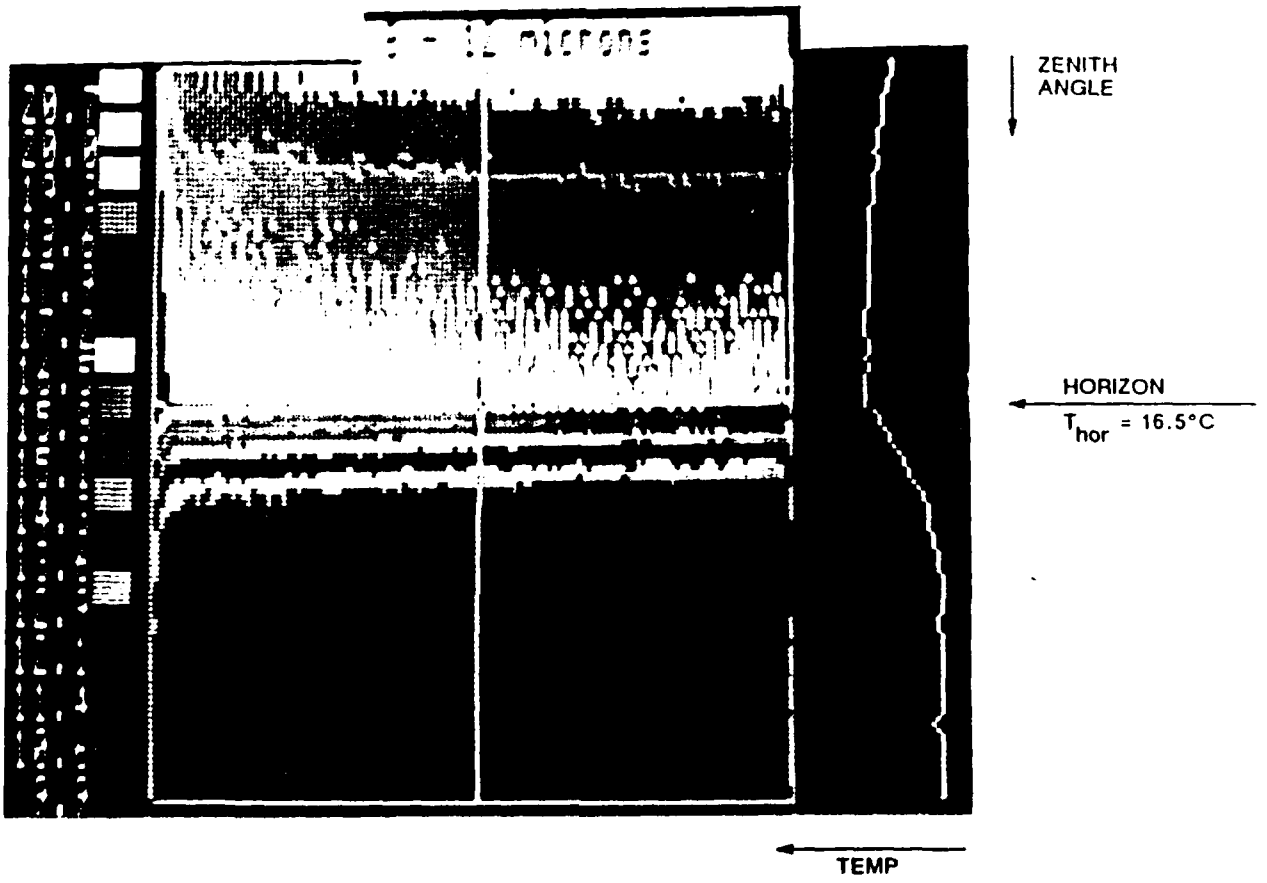

Figure 3. Thermogram of near horizon infrared (8 to 12 μm) radiances measured over the ocean by an AGA THERMOVISION Model 780 thermal imaging system on 9 June 1988.

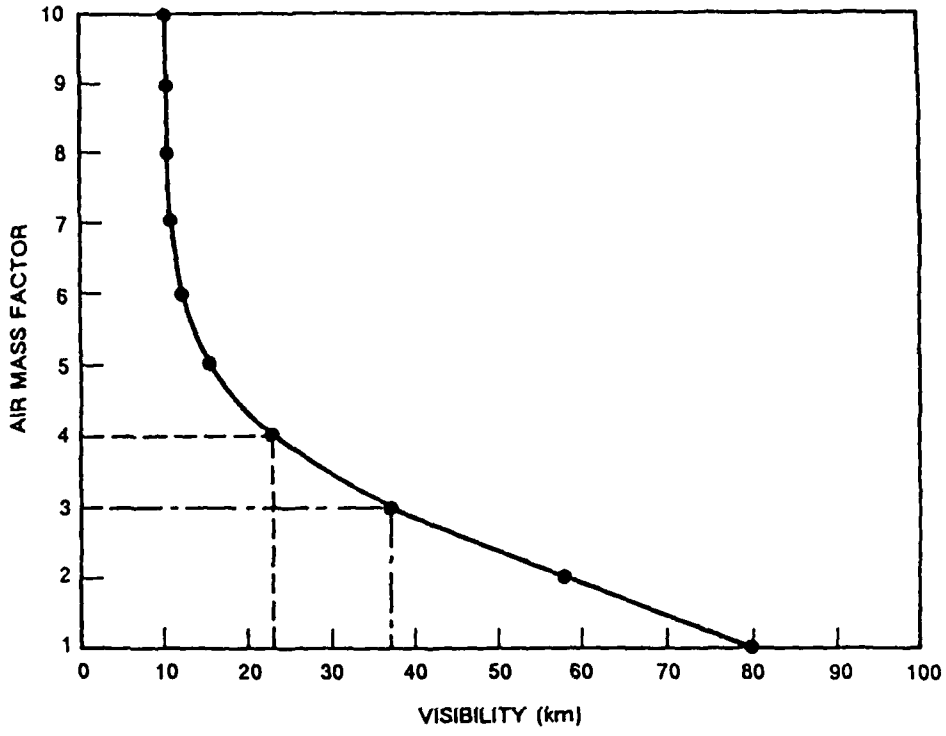

Figure 4. Locus of points of LOWTRAN 6 calculations with different combinations of air mass factors and visibilities which match the measured infrared horizon radiance in figure 3.

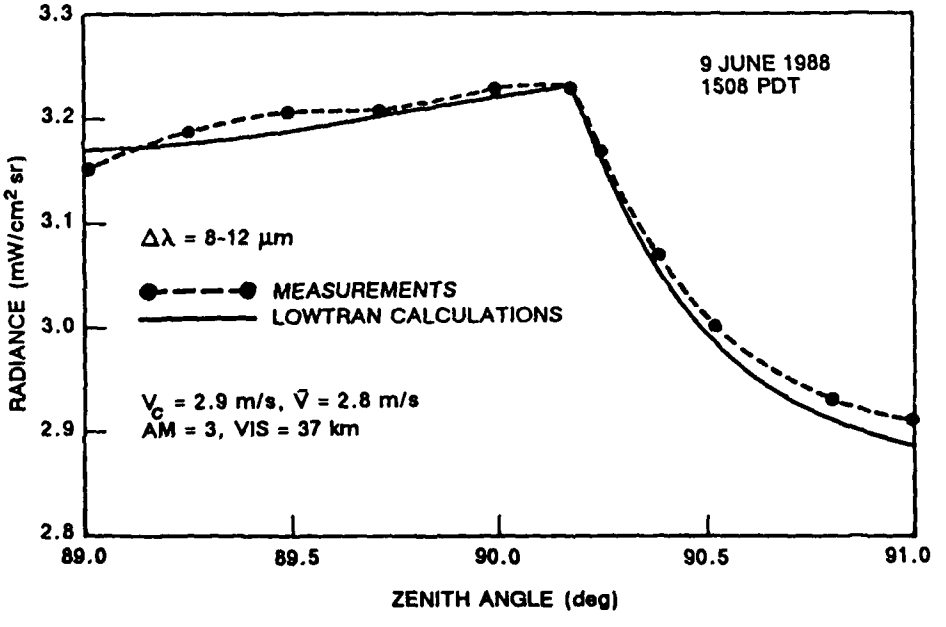

Figure 5. Comparison of measured and calculated infrared radiances for zenith angles above ($\theta < 90.17°$) and below ($\theta > 90.17°$) the horizon.

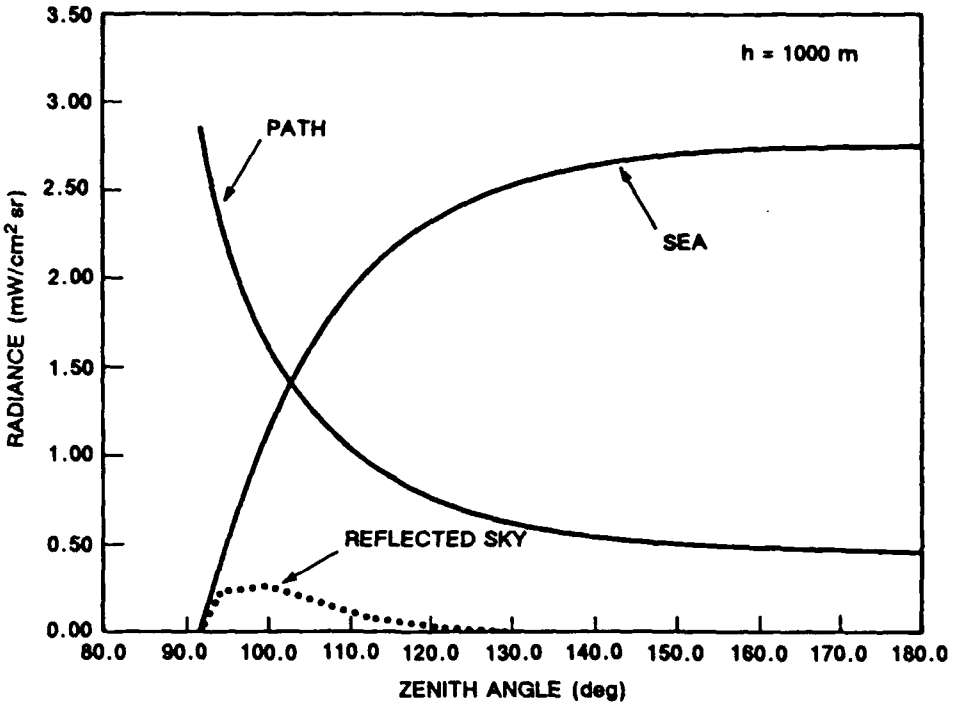

Figure 6. Individual contributions of the path, sea and reflected sky radiances to the total background radiance as a function of zenith angle for a sensor altitude of 1000 m.

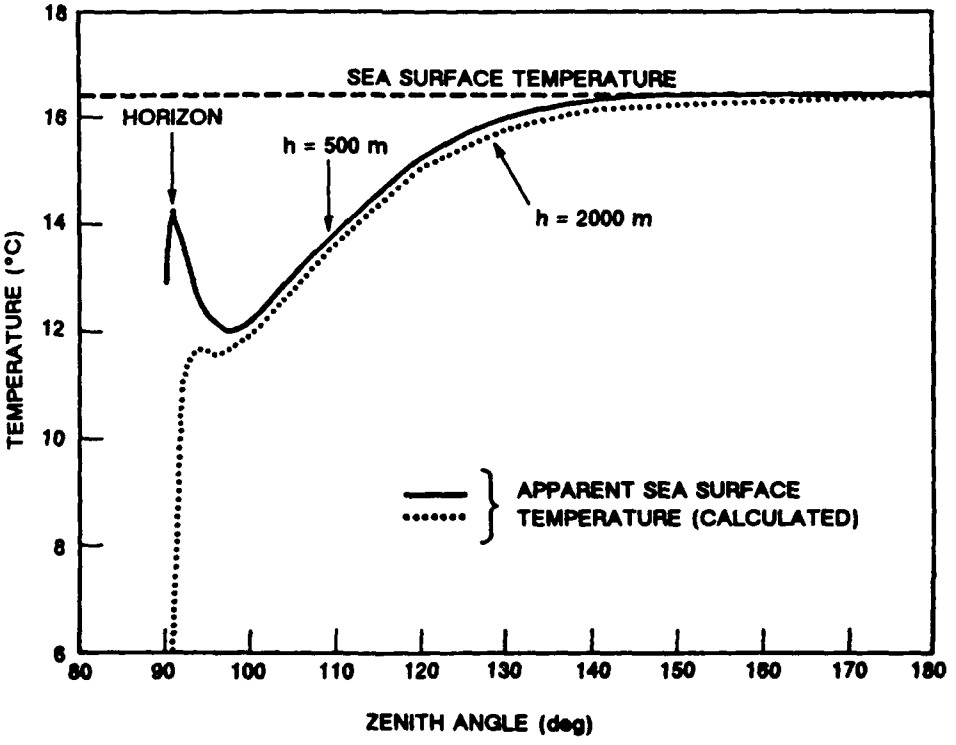

Figure 7. Total apparent blackbody temperature of the sea background versus zenith angle for sensor altitudes of 500 m and 2000 m.

AVERAGED SHIP TEMPERATURE MODEL

The computer code SHIPSIG (Ostrowski and Wilson, 1985) for predicting the average temperature of a surface vessel was developed at the Naval Surface Weapons Center. The original BASIC version of the code has been rewritten in FORTRAN language for the HP-9020 computer. Basically, the model approximates the complex structure of a ship with a single-plane element which represents the ship on an average basis. For a given viewing direction, the simplest representation of a ship consists of a single vertical element and a horizontal element with the observer's orientation accounted for by appropriate area components. The infrared signature calculations are then based on a thermodynamic analysis of both elements individually. They are combined by scaling the element radiance in proportion to the ship area each represents. The thermodynamic properties of the horizontal and vertical elements and ship stack correction factors applied to the vertical element presently listed in the SHIPSIG code are for a guided-missile, frigate-class ship. The model requires as inputs the ship's course and speed as a function of time from a starting geographic latitude, the surface wind speed and direction, visibility, relative humidity, air temperature, the ship's initial temperature, and the viewing angle.

Figure 8 shows the course of a guided-missile frigate, the USS *Brooke* (FFG 1), chosen to demonstrate the model off the coast of San Diego on 9 June 1988. During the 5-hour period, changes in the ship's heading allowed solar heating of different sides of the ship. As the ship completed the course and returned to harbor, it passed close to the the AGA thermal imaging system located on shore about 2 km from channel buoy #6 near the entrance to the harbor.

Figure 9 is the thermogram taken with the AGA system as the ship entered the harbor. The ship in the top figure is the *Brooke* (FFG 1) and the ship at the bottom is the *Crommelin* (FFG 37). The course history of the *Crommelin* was not available; however, both ships had been on a joint midshipman training exercise and had operated in the same area.

The AGA system's data processing software allows subtraction of the sea background radiance surrounding the ships and provides a histogram of the temperature distribution of the ship pixels within the chosen rectangular area, as shown in the inset to the right of each ship. Temperatures on the histogram (percentage of total number of pixels in a temperature band) are shown in the color corresponding to the bar on the temperature scale to the left. The mean temperature (uncorrected for atmospheric effects) was 19.7°C for both ships, which is rather surprising since they are equipped with different types of power plants (i.e., steam power for the *Brooke* versus gas turbines for the *Crommelin*). Superimposed on each histogram is a Gaussian curve (represented by dots) which best fits the temperature points. In both cases, the temperature distributions approximate the Gaussian curves remarkably well. The measured radiance, N(meas), of the ship at a range R is related to its actual effective blackbody radiance, N(ship), and the atmospheric emission, N(path), along the path by

$$N(meas) = N(ship)\tau(R) + N(path) \qquad (12)$$

where $\tau(R)$ is the atmospheric transmittance at a range R. The range to the ship was determined to be approximately 1.7 km using the known vertical dimensions of the

ship and their angular subtense within the field of view of the AGA. The relative humidity (72 percent), air temperature (20°C), and pressure (1012.4 mb) measured at the AGA location were used in LOWTRAN 6 calculations of transmittance and path emission to determine the temperature equivalent to N(ship). Figure 10 shows the adjusted temperature dependence on visibility and air mass factor. Conveniently, both of the combinations of air mass factor and visibility (AM = 3, visibility = 37 km; and AM = 4, visibility = 23 km) result in the same adjusted ship's temperature of 20.5°C.

For the model calculations, the initial position of the ship was taken to be near the entrance to San Diego harbor. The initial ship temperature, its ambient temperature, and relative humidity throughout the course were not recorded by the ship. The relative humidity was then taken to be constant as measured at the AGA site. The surface wind was southwesterly at 2.9 m/s and the visibility was taken as 37 km. The depression angle of viewing was 0.6°. The average ship temperature calculated for the port side of the ship as a function of time is shown in figure 11, assuming the initial ship temperature to be equal to the indicated ambient air temperatures which remained constant throughout the cruise. The most apparent feature is the ship's temperature response to the gradual heating of its port side as it steamed westward in the early morning and the abrupt cooling after 1000 hours, following the southeasterly course change at 0952 hours. While the shapes of the response curves do not appear sensitive to the uncertainties in ambient air temperature, their magnitudes differ by amounts equivalent to the uncertainties. Allowing for the uncertainties in the meteorological parameters surrounding the ship throughout the course, the reasonable agreement between the adjusted AGA temperature measurements near 1345 hours and the model is gratifying.

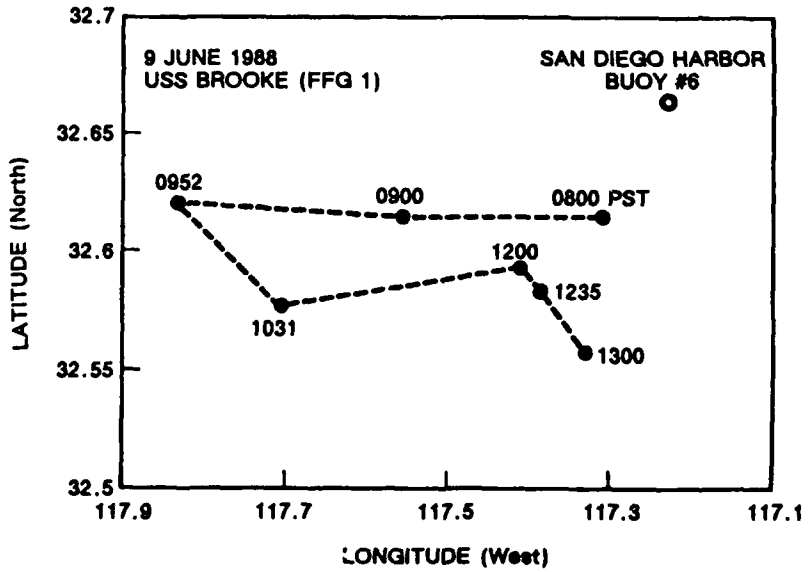

Figure 8. Course of the USS *Brooke* (FFG 1) on 9 June 1988.

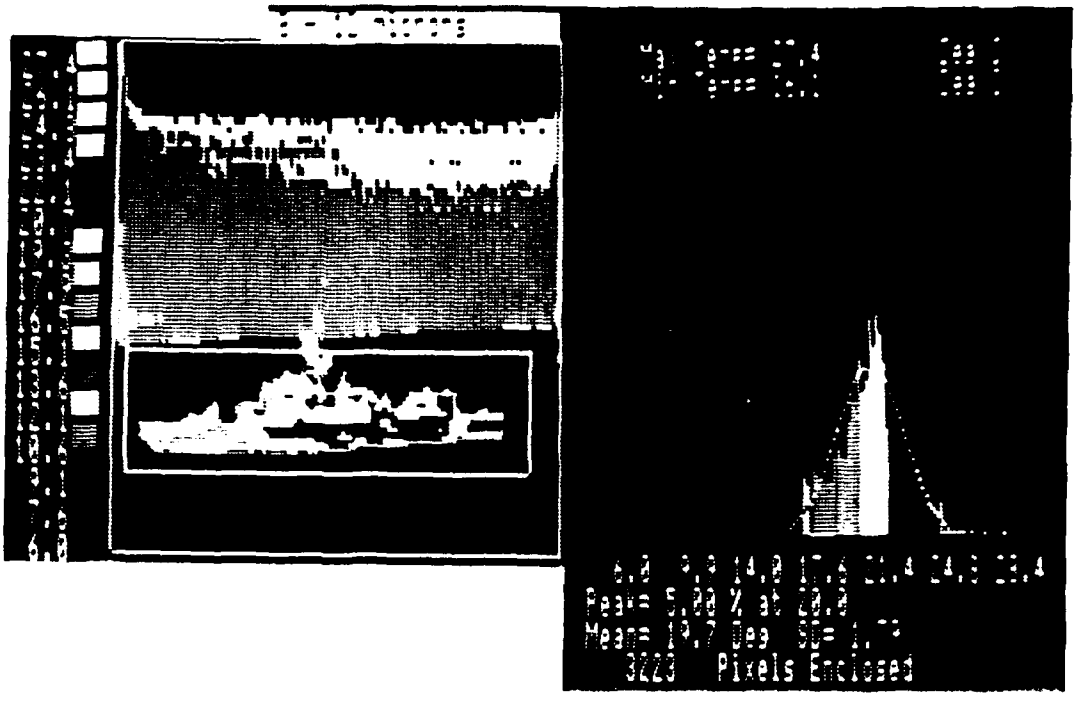

USS BROOKE (FFG 1)
1354 PST

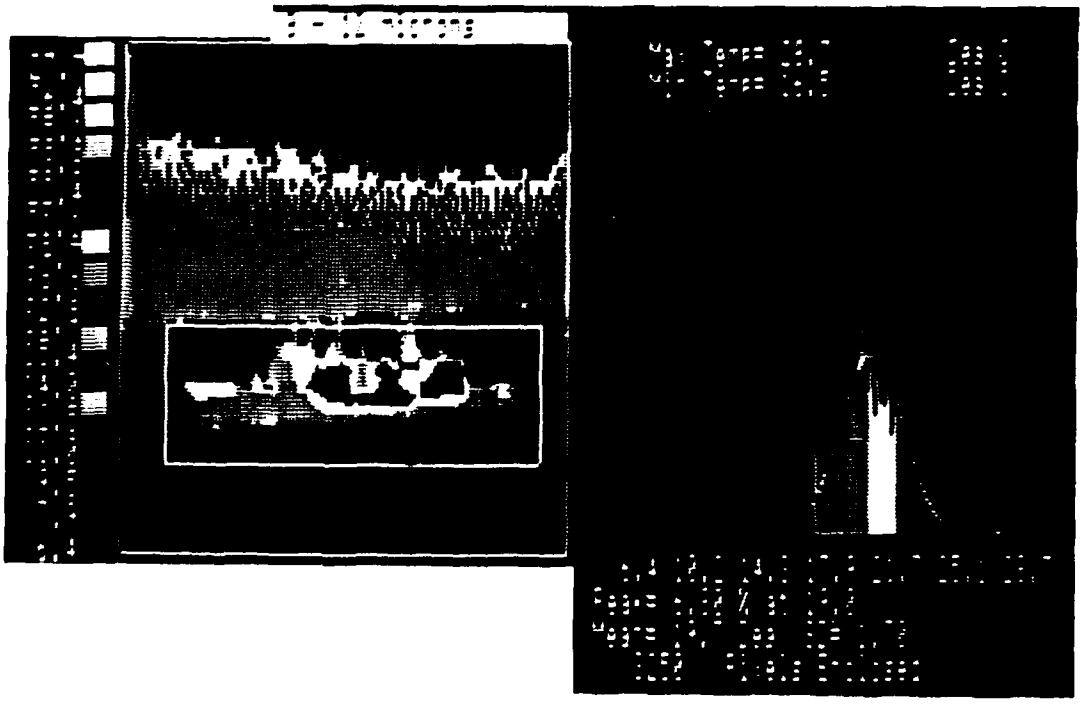

USS CROMMELIN (FFG 37)
1400 PST

Figure 9. Infrared thermograms of the USS *Brooke* (FFG 1) and the USS *Crommelin* (FFG 37) as they entered San Diego harbor on 9 June 1988.

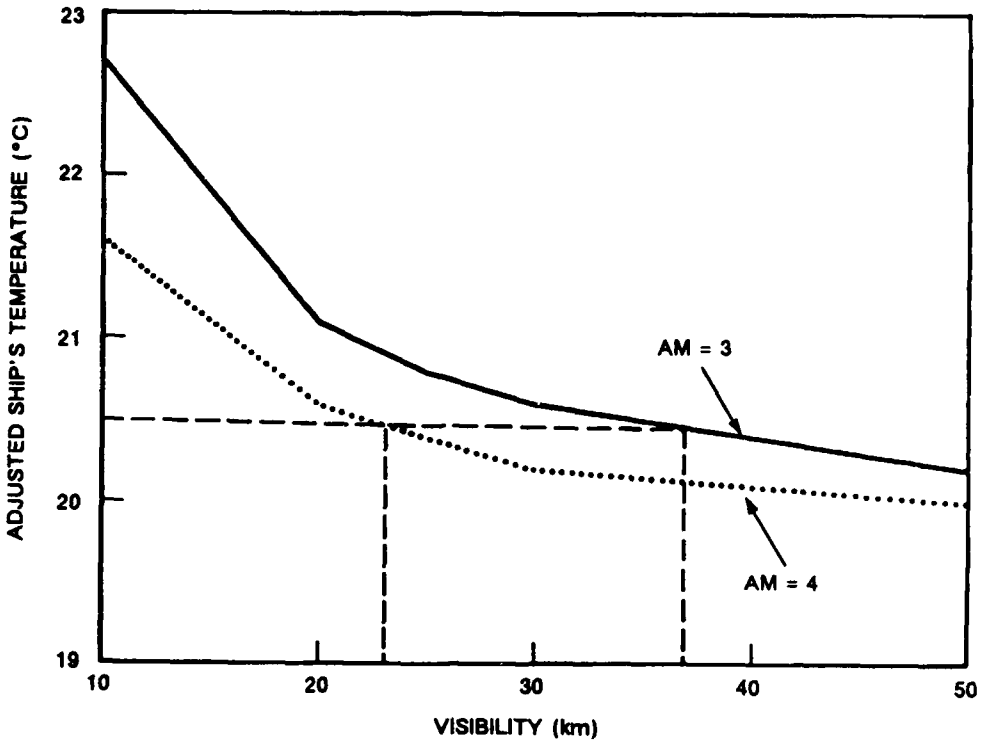

Figure 10. Ship's average temperature adjusted for atmospheric effects versus visibility for different AM factors.

DETECTION RANGE CALCULATIONS

The concept of maximum detectable range (MDR) calculations using a fixed difference between a target at a temperature, T_s, and its effective background temperature, T_b, is depicted in figure 12. The MDR is defined as that range where the actual temperature difference ($T_s - T_b$) is degraded by the atmospheric transmittance, $\tau(R)$, to an apparent temperature difference, ΔT_a, equal to the minimum detectable temperature difference (mdtd) of the system. As stated earlier, this approach neglects effects of a wind-ruffled sea on the surface emissions and sky reflections and the atmospheric path emissions which contribute to the total background scene under cloud-free skies. It also neglects the path radiance between the target and detector, which must be accounted for in a temperature difference concept for detection range predictions. The radiance contrast between a ship and its

background can be converted to an equivalent temperature difference if the slope of the radiance gradient with temperature is specified, i.e.,

$$(N_s - N_b)/(T_s - T_b) = \partial N/\partial_{T=T'} \tag{13}$$

or,

$$\Delta T_{eq} = \frac{\Delta N}{\partial N/\partial_{T=T'}} \tag{14}$$

where the wavelength dependency of N is implied. The equivalent temperature difference is somewhat sensitive to the choice of the temperature, T', at which the gradient is chosen. For the 8- to 12-μm wavelength band, the gradient at 280°K is approximately 11 percent lower than that at 290°K and 27 percent at 310°K (Lloyd, 1975).

In the calculations presented here, the unmodified LOWTRAN 6 code is used to directly calculate the sum of the ship and path radiances received by the sensor at a range R as

$$N(R)_{s+p} = N(R=0)_s\tau(R) + N(R)_p \ . \tag{15}$$

$N(R)_{s+p}$ is then converted to an equivalent blackbody temperature $T(R)_{s+p}$ by an iterative solution to Planck's blackbody formula. Similarly, an equivalent blackbody temperature, $T(R)_b$, of the background radiance (equation 12) at the specified range is calculated and the resulting apparent temperature difference , $\Delta T(R)_a = T(R)_{s+p} - T_b$, determined. As shown in the inset of figure 11, the intersection of the curve of $\Delta T(R)_a$ plotted versus range with that of the system's mdtd curve determines the MDR of the ship. The FLIR system mdtd versus range (spatial frequency) curve was calculated using the formulation for a hypothetical FLIR operating against a rectangular target. In figures 13 and 14, the calculated MDRs for the *Brooke* by an airborne FLIR operating at altitudes of 0.5 and 1.0 km, respectively, are shown. The MDRs could have been calculated as a function of time throughout the the ship's course; however, for the sake of simplicity, only the vulnerability detection envelopes for the entire duration of the ship's course are shown. In the figures, the ship's average temperatures for both the port and starboard sides are shown. In figure 13, the ship is seen to be vulnerable to IR detection throughout its course from an altitude of 0.5 km at a range of 31 km. However, beyond 35 km the ship is not detectable. Similarly, in figure 14, the ship is vulnerable at a range of 53 km from an altitude of 1.0 km, but safe from detection at 56 km. In these examples, note that the temperature responses of the different sides of the ship to solar heating follow the course changes remarkably well. In figure 15, comparison is shown of the predicted detection ranges using the present algorithm and those assuming a constant temperature difference between the ship and its background of 5°C (CSC, 1986). Considerable increases (≈20 km at an altitude of 2.0 km) in predicted detection ranges with altitude are obtained using the present method over the fixed-temperature method.

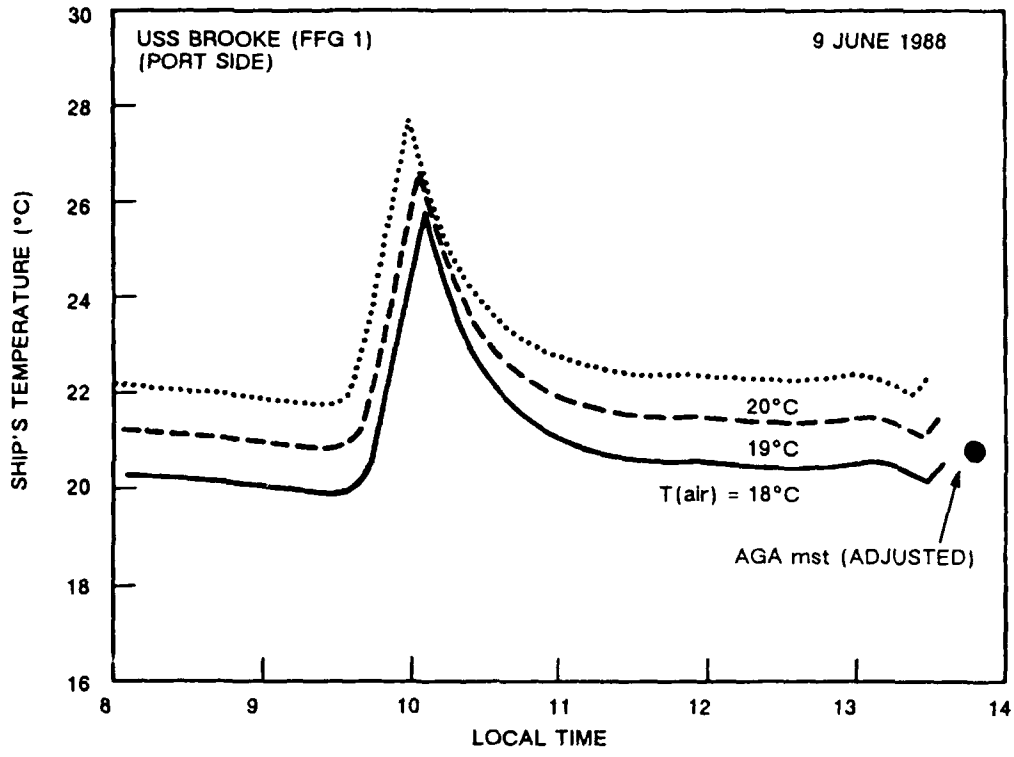

Figure 11. Comparison of the average temperatures of the port side of the USS *Brooke* (FFG 1) (calculated using different ambient air temperatures) with the adjusted AGA measurements as the ship entered San Diego harbor.

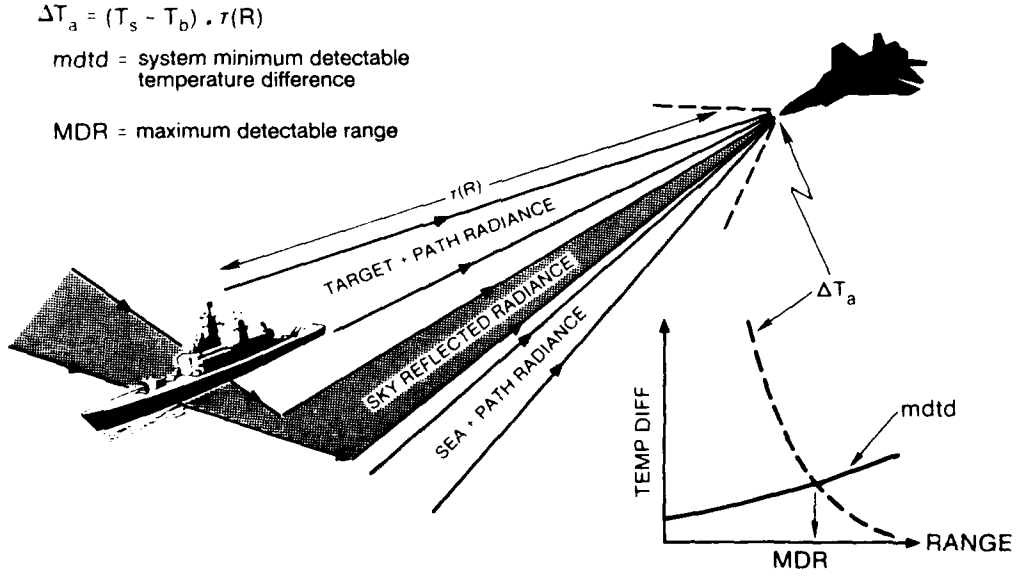

Figure 12. Illustration of the detection of a surface target by an airborne FLIR system.

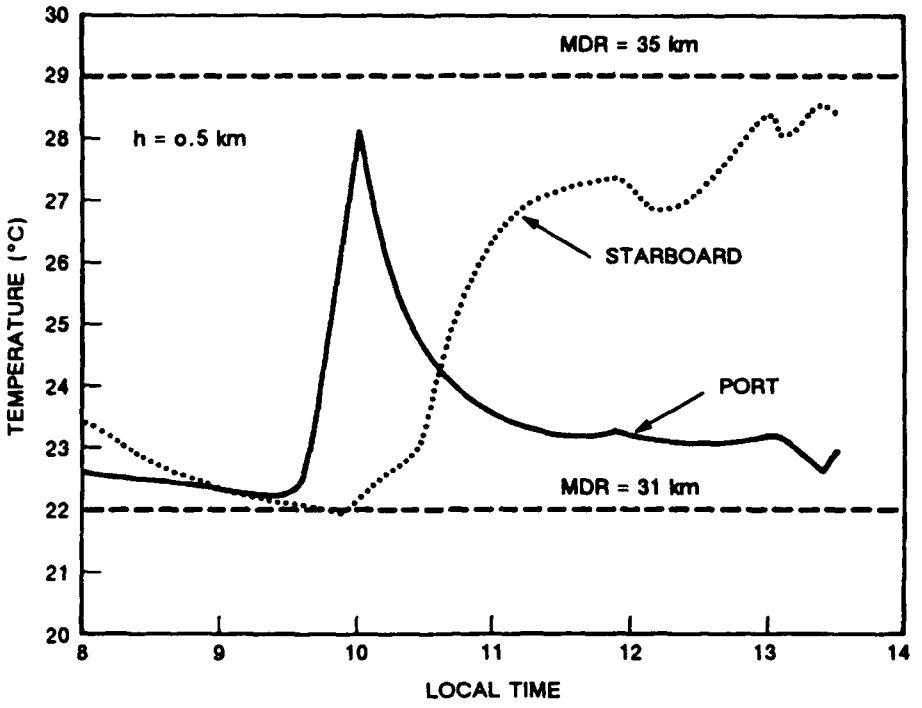

Figure 13. Calculated MDR envelopes for the USS *Brooke* (FFG 1) by an airborne FLIR at an altitude of 0.5 km.

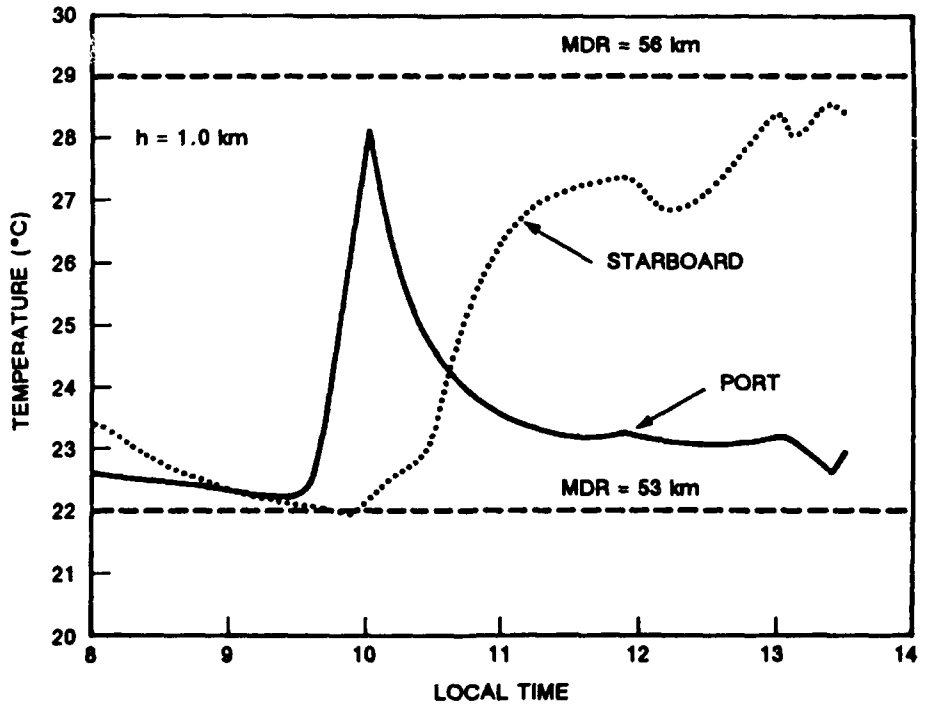

Figure 14. Calculated MDR envelopes for the USS *Brooke* (FFG 1) by an airborne FLIR at an altitude of 1.0 km.

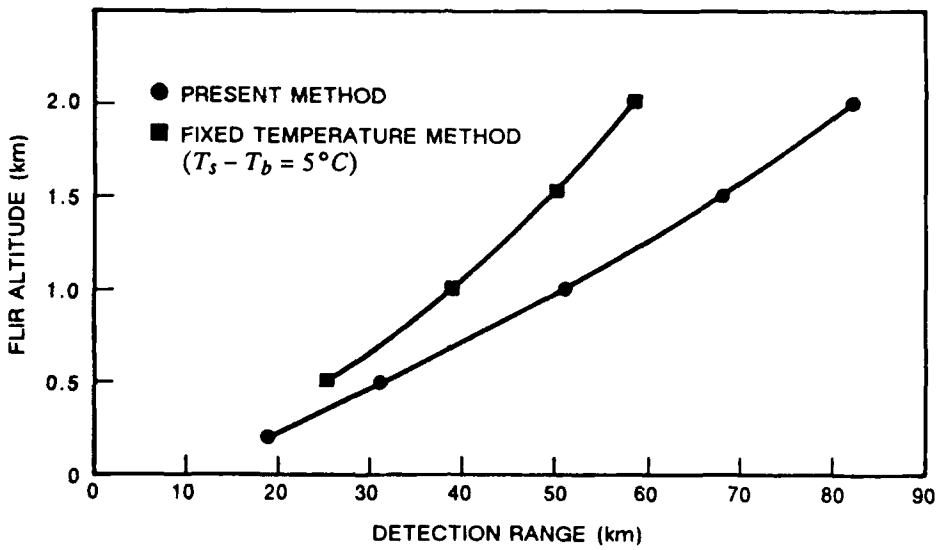

Figure 15. Comparison of the maximum detectable ranges (lower envelope) for the USS *Brooke* (FFG 1) calculated with the present algorithm and those calculated assuming a constant temperature difference of 5°C between the ship and its background.

CONCLUSIONS AND RECOMMENDATIONS

The results of this case study have shown the reliability of the sea-surface radiance model to accurately represent measured values for a low-wind-speed condition. Whether or not it will be representative of other wind-speed conditions should be determined. Also, the preliminary evaluation of the average ship temperature model showed promise that it responds to the differing solar conditions. Future attempts at validation should ensure the accuracy of the ambient meteorological conditions. On-board ground-truth radiometry measurements of the temperatures of different portions of the ship are also needed to aid in determining the accuracy of the adjusted average temperatures inferred from the AGA measurements. Finally, a controlled experiment with an airborne operational system should be conducted to determine the validity of the predicted detection ranges under varying meteorological conditions.

REFERENCES

Computer Sciences Corporation (1988). *Forward Looking Infrared Performance Function Program Performance Specification (PPS) for the Tactical Environmental Support System (TESS)*. NOSC TD 1000.

Cox, C., and W. Munk (1954). "Measurement of Roughness of the Sea Surface from Photographs of the Sun's Glitter," *Jour. Opt. Soc. of Am.*, 44, 838.

Hughes, H.G. (1987). "Evaluation of the LOWTRAN 6 Navy Maritime Aerosol Model Using 8- to 12-μm Sky Radiances," *Opt. Eng.*, 26, 1155.

Kneizys, F.X., E.P. Shettle, W.O. Gallery, J.H. Chetwynd, Jr., J.H. Abreu, J.E.A. Selby, S.A. Clough, and R.W. Fenn (1983). *Atmospheric Transmittance/ Radiance: Computer Code LOWTRAN 6*. Air Force Geophysics Laboratory Technical Report No. 83-0187.

Lloyd, J.M. (1975) *Thermal Imaging Systems*. Plenum Press New York, p. 28.

Ostrowski, P.P., and D.M. Wilson (1985). *A Simplified Computer Code for Predicting Ship Infrared Signatures*, NSWC TR 84-540.

STX Corporation (1988). *FLIR Program Upgrade–Users Manual*. NEPRF Document RW0513, UM-40.

Wollenweber, F.G. (1988). *Effects of Atmospheric Model Layering on LOWTRAN 6 Calculations of 8- to 12-μm Near Horizon Sky Radiances*, NOSC TD 1193.

Wollenweber, F.G. (1988). *Infrared Sea Radiance Modeling Using LOWTRAN 6*, NOSC TD 1355.